Appl. Phys. B 80, 861–864 (2005)
DOI: 10.1007/s00340-005-1810-9

Applied Physics B
Lasers and Optics

E. SAMSØE[1,2]
P.M. PETERSEN[1]
S. ANDERSSON-ENGELS[2]
P.E. ANDERSEN[1,✉]

Second-harmonic generation of 405-nm light using periodically poled $KTiOPO_4$ pumped by external-cavity laser diode with double grating feedback

[1]Department of Optics and Plasma Research, Risø National Laboratory, 4000 Roskilde, Denmark
[2]Department of Physics, Lund Institute of Technology, 221 00 Lund, Sweden

Received: 14 October 2004 / Revised version: 8 March 2005
Published online: 3 May 2005 •

ABSTRACT A frequency-doubled laser diode system for generation of blue–UV light is described. The system is based on an external-cavity high-power laser diode with double feedback from the zeroth and the first orders of a diffraction grating. Light at 405 nm is generated in a single-pass configuration using periodically poled $KTiOPO_4$. We show that the double grating feedback improves the second harmonic conversion efficiency by several orders of magnitude as compared to the freely running laser. The conversion efficiency may be improved further such that higher second-harmonic powers may be generated.

PACS 42.55.Px; 42.60.Jf; 42.65.Ky

1 Introduction

Compact laser sources in the blue–UV spectral region are feasible for use in many of today's photonics applications, such as optical storage and biomedicine. Quasi-phase-matched second-harmonic generation (SHG) is an attractive method for generating blue light. The main advantage of quasi-phase matching (QPM) is the possibility of using the larger nonlinear elements in the diagonal of the $\chi^{(2)}$ tensor, which are not accessible to birefringent phase matching. Another major advantage of QPM is that noncritical phase matching may be used at any wavelength within the transparency range of the nonlinear material by appropriate choice of the period for the domain inversion. High-power laser diodes (LDs) are preferred in many applications due to their compactness, low cost, and high efficiency. However, they suffer from poor spatial and temporal coherence and are thus not suitable for applications requiring a well-focused beam with narrow spectral bandwidth, such as SHG. Several schemes have been proposed in order to implement high-power LDs as pump sources in SHG. Complicated systems such as master oscillator power amplifiers (MOPAs) [1] or more simple external cavities using single-mode LDs [2] may be used. Remaining drawbacks are complexity and low power, respectively. Single-pass SHG using high-power LDs, such as multiple-stripe lasers or broad-area lasers, has not been successful due to the poor spatial and temporal coherence of such lasers. However, these lasers are important for pumping solid-state lasers, which then act as sources for frequency doubling. Direct emission at short wavelengths is available with the InGaN-based laser diode [3] at 405 nm. However, this wavelength is fixed by the material band gap and, moreover, further improvement of the device lifetime is required.

In this article, we present the first experimental results from frequency doubling the output of a double grating feedback (DGF) laser [4], thereby generating light at 405 nm. We recently demonstrated this external cavity for improving both the spatial and the temporal coherence of high-power, broad-area laser (BAL) diodes. The setup uses double feedback from the zeroth reflected order and the first diffracted order of a diffraction grating in addition to spatial filtering. For the SHG, we use a first-order, periodically poled $KTiOPO_4$ (PPKTP) crystal arranged in a single-pass configuration. The results are compared to the predictions from Boyd–Kleinman theory [5] and to an extended theory for elliptical beams [6]. We show that the double grating feedback improves the second harmonic conversion efficiency by several orders of magnitude as compared to the freely running laser. Initial experiments indicate that the power may be increased significantly by pulsing the pump laser [7]. The system has the long lifetime of the GaAs-based LDs and is not limited to 810-nm/405-nm operation.

2 Experiment

The experimental setup is illustrated in Fig. 1a–c. Figure 1a illustrates the generation of far-field image planes using the collimating optics and Fig. 1b and c present a side view and a top view, respectively, of the setup. The purpose of this setup is to allow simultaneous feedback from both the zeroth reflected order and the first diffracted order.

The BAL is mounted with its high-coherence axis (fast axis) parallel to the transverse direction (y axis) and its

✉ Fax: +45-4677-4588, E-mail: peter.andersen@risoe.dk

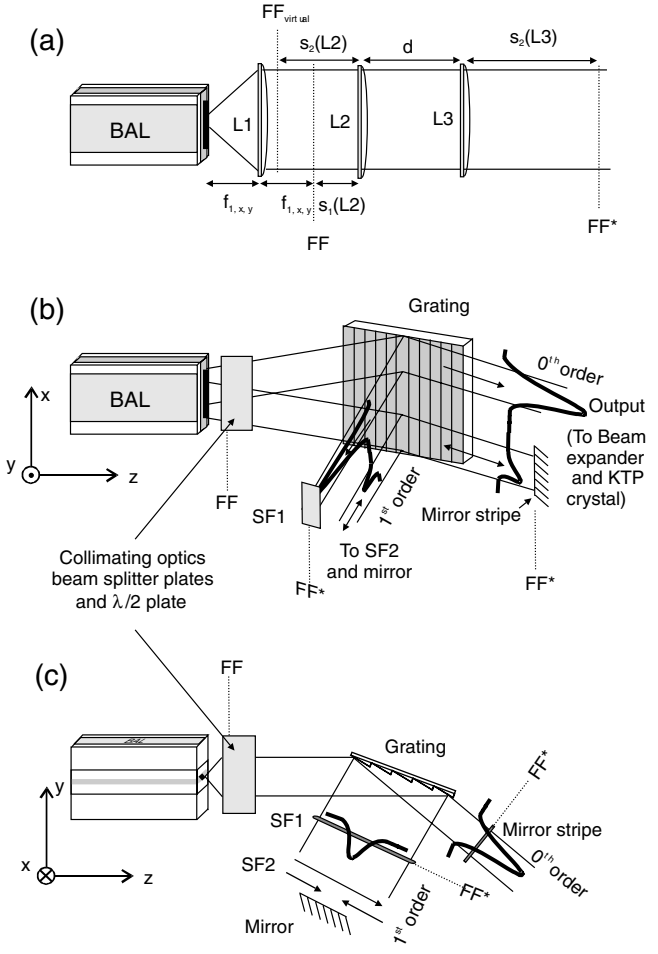

FIGURE 1 Collimation and generation of image planes (**a**), side view (**b**), and top view (**c**) of experimental setup [4]. BAL: broad-area laser; Li: collimating lenses; $f_{1,x}$: focal length of L1; s_1(Li): distance from object plane to Li; s_2(Li): distance from Li to image plane; FF: lateral far-field plane; $FF_{virtual}$: virtual image plane of FF; FF*: image plane of FF; SF1: spatial filter in the lateral direction; SF2: spatial filter in the transverse direction; x, y, and z: lateral, transverse, and longitudinal directions, respectively. The shapes of the intensity profiles are outlined in *black*

low-coherence axis (slow axis) parallel to the lateral direction (x axis). The output is collimated using three anti-reflection (AR)-coated lenses, L1–L3. L1 is inserted at a focal length distance from the BAL emission facet, thereby collimating the transverse direction. At the same time L1 generates a far-field plane, FF, for the lateral direction in its front focal plane. The lenses L2 and L3 collimate the beam in the lateral direction and generate an image of the far-field plane, FF, in the plane(s) FF* at distance(s) s_2(L3) from L3. The distance s_2(L3) is determined by the distances between FF, L2, and L3 through the lens-maker's equation [8]:

$$\frac{1}{s_1}+\frac{1}{s_2}=\frac{1}{f}, \tag{1}$$

where s_1 is the distance from the object, i.e. the intensity distribution in FF, to the lens with focal length f, and s_2 is the distance from the lens to the image plane of FF, i.e. FF*. L1 is an aspheric lens with focal length $f_{1,xy}=4.5\,\text{mm}$ and a numerical aperture NA = 0.55. L2 and L3 are cylindrical lenses with focal lengths $f_{2,x}=10\,\text{mm}$ and $f_{3,x}=60\,\text{mm}$, respectively. With L2 placed at a distance $s_1(\text{L2})=4\,\text{mm}$ from FF, a virtual image of FF is generated in the plane $FF_{virtual}$ at a distance $s_2(\text{L2})=-6.7\,\text{mm}$ from L2. The third lens, L3, is inserted at a distance $d=76\,\text{mm}$ from L2, i.e. $s_1(\text{L3})=d-s_2(\text{L2})=82.7\,\text{mm}$, which yields an image plane, FF*, at a distance $s_2(\text{L3})=219\,\text{mm}$ from L3. This image occurs in both orders as depicted in Fig. 1b and c.

A $\lambda/2$ plate is inserted to rotate the polarization by 90° such that the light incident on the grating is TE-polarized parallel to the grating grooves (x direction). This choice of polarization leads to a low diffraction efficiency and thus optimizes the amount of power in the zeroth-order output beam. The diffraction grating with 1200 lines/mm is arranged such that the incident beam enters the grating at an angle of $\theta_{in}=72°$ with respect to the grating normal $\vec{n}$. The angular dispersion of the light is optimized by inserting the grating at a large angle, thereby illuminating the entire width of the grating. This minimizes the single-pass bandwidth $\Delta\lambda$ of the output light at wavelength λ.

Two orthogonal spatial filters, SF1 and SF2, are inserted in the first-order beam between the grating and the mirror. The filters select parts of the beam to pass through in the lateral (SF1) and transverse (SF2) directions, respectively. Only a narrow wavelength band is reflected back along the direction of incidence on the mirror, the wavelength depending on the mirror orientation due to the dispersive and filtered feedback. This back-reflected beam is diffracted again by the grating and is returned to the BAL. The zeroth order of this second diffraction is lost. However, the higher diffraction efficiency at this small angle of incidence results in a negligible loss in the order of 1 mW. SF1 is placed in the image plane of the far-field plane, FF*. At this same distance, but in the zeroth order, a mirror stripe is inserted to provide feedback to the laser and thereby to control the spatial emission profile. The lateral filter in the first order and the mirror stripe in the zeroth order are matched to allow for the same spatial parts of the beam, the small lobe, to be reflected. When the mirror stripe in the zeroth order is illuminated, the far field changes from a broad radiation pattern to the well-known asymmetric double-lobe pattern [9]. This allows that one of the lobes is used for the feedback by the mirror stripe, while the other serves as the output beam. When the mirror and the transverse filter, SF2, in the first order are correctly aligned, the spectrum narrows significantly. When allowing for feedback from the zeroth order in addition, and when the lateral filter in the first order matches the position of the mirror filter in the zeroth order, the spectrum becomes even narrower and more intense.

The output is 3.6 times the diffraction limit with a spectral bandwidth of $\Delta\lambda=0.08\,\text{nm}$ (FWHM) when DGF is applied. At $T=44°\text{C}$ and $I=1400\,\text{mA}$ ($=2.4I_{th}$) we obtain an output power of 445 mW at 810 nm corresponding to 54% of the power from the freely running, collimated BAL. The elliptical output beam is expanded in the slow-axis direction, using two AR-coated cylindrical lenses ($f_{cyl,1}=10\,\text{mm}$ and $f_{cyl,2}=60\,\text{mm}$). The expanded output is focused into the nonlinear crystal with an $f=100\,\text{mm}$ plane-convex lens. The elliptical spot measures $w_x\times w_y=75\,\mu\text{m}\times 20\,\mu\text{m}$, where w_x and w_y are the beam waists (radii at $1/e^2$) in the slow and fast axes, respectively. The power available for pumping the nonlinear crystal is 405 mW. The PPKTP crystal is 10-mm

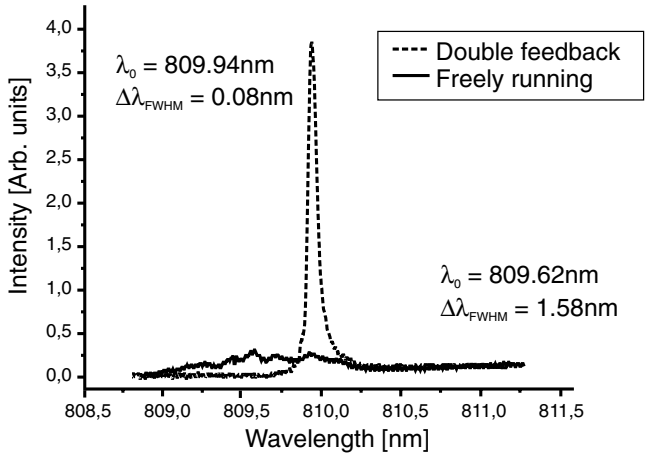

FIGURE 2 Spectral characteristics of pump laser with and without double grating feedback from first and zeroth orders of a diffraction grating

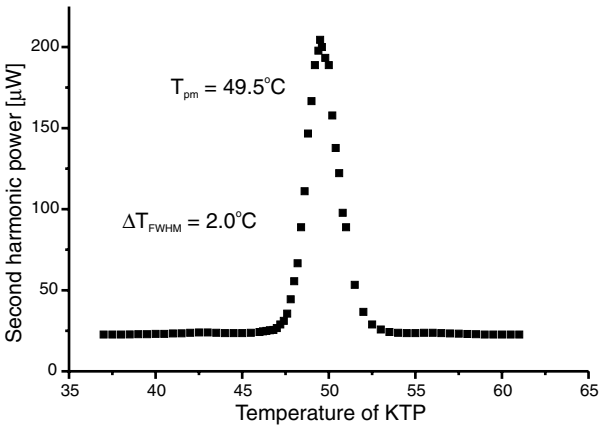

FIGURE 4 Temperature-tuning curve of the PPKTP crystal measured with the DGF laser

long, AR coated for 810 nm/405 nm, with a grating period of $\Lambda = 3.4\,\mu\text{m}$ and an aperture of $1 \times 2\,\text{mm}^2$. The acceptance bandwidth of the crystal has been stated by the manufacturer (private communication) to be 0.07–0.08 nm. A dichroic beam splitter separates the fundamental from the second-harmonic output. The spectral characteristics at $I = 2.4I_{\text{th}}$ of the DGF laser are shown in Fig. 2. The spectral bandwidth improves from $\Delta\lambda = 1.6\,\text{nm}$ to $\Delta\lambda = 0.08\,\text{nm}$ when double feedback is applied.

3 Results and discussion

Figure 3 shows the measured second-harmonic power as a function of fundamental power with and without DGF. The results without DGF are measured when the first-order feedback path is blocked so that the LD only receives zeroth-order feedback (ZOF), i.e. only the spatial coherence of the LD is distinctly improved. The lines represent a fitted quadratic curve to the measurements according to [5]

$$P_{2\omega} = \frac{16\pi^2 d_{\text{eff}}^2}{\epsilon_0 c \lambda_\omega^3 n_{2\omega} n_\omega} L h(B,\xi) P_\omega^2, \tag{2}$$

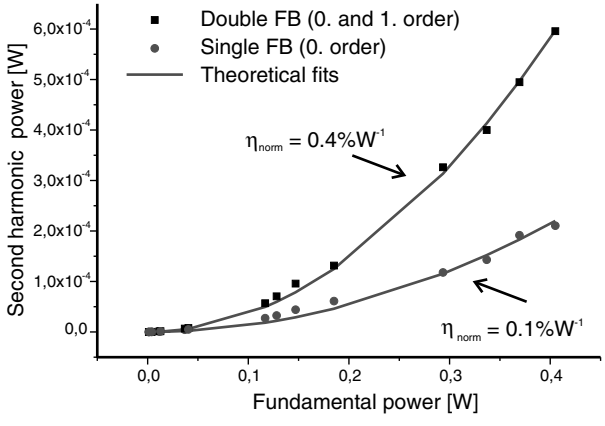

FIGURE 3 Second-harmonic power as a function of fundamental power. The *squares* are for the DGF laser and the *dots* are measured with the single-feedback laser with zeroth-order feedback only

where we neglect the linear absorption and where ϵ_0 is the permittivity of free space, λ_ω is the fundamental wavelength, $n_{2\omega}$ and n_ω are the refractive indices at the second-harmonic and the fundamental frequencies, respectively, d_{eff} is the effective nonlinear coefficient, L is the (effective) crystal length, $h(B,\xi)$ is the Boyd–Kleinman focusing factor [5], and P_ω is the power of the fundamental beam. In our case, there is noncritical phase matching and $B = 0$. The focusing parameter is $\xi = L/b$, where b is the confocal parameter. With an average waist size of $w_0 = \sqrt{w_x w_y} = 39\,\mu\text{m}$, we obtain $h(B,\xi) = h(0, 0.25) = 0.27$ from Ref. [5]. The effective nonlinear interaction length may be estimated from the temperature-tuning curve [10], which was measured and is shown in Fig. 4. The temperature-tuning bandwidth can be expressed as [11]

$$\Delta T_{\text{FWHM}} = \frac{1.39\lambda}{\pi L} \left| \frac{\partial n_{2\omega}}{\partial T} - \frac{\partial n_\omega}{\partial T} \right|^{-1}, \tag{3}$$

assuming a perfect periodic poling of the crystal. The refractive indices, $n_{2\omega} = n_{2\omega,z} \approx 1.96$ and $n_\omega = n_{\omega,z} \approx 1.84$ (type I phase matching), and the refractive-index temperature derivatives, $\partial n_{2\omega}/\partial T \approx 50.0 \times 10^{-6}\,(^\circ\text{C})^{-1}$ and $\partial n_\omega/\partial T \approx 16.6 \times 10^{-6}\,(^\circ\text{C})^{-1}$, are calculated from Ref. [12]. The temperature-tuning bandwidth was determined to be $\Delta T_{\text{FWHM}} = 2.0^\circ\text{C}$, which corresponds to an effective nonlinear interaction length of $L_{\text{eff}} = 5.4\,\text{mm}$ using Eq. (3). The discrepancy between the effective nonlinear interaction length and the physical length of the crystal is attributed to the spectral width of the pump laser and may also be due to imperfections in the grating structure of the crystal.

Without external feedback, the second-harmonic power is below the minimum detectable power (1 μW) for our detector. When the feedback circuit that improves the spatial coherence is applied, a maximum second-harmonic power of 0.2 mW corresponding to a normalized conversion efficiency of $P_{2\omega}/P_\omega^2 = \eta_{\text{norm}} = 0.1\%\,\text{W}^{-1}$ is measured. This number is improved to $\eta_{\text{norm}} = 0.4\%\,\text{W}^{-1}$, or 0.6 mW, when both feedback circuits are applied. The DGF thus improves the conversion efficiency by several orders of magnitude as compared to the freely running laser. The blue output power exhibits a stable behaviour with a deviation from the mean power of ±5% during a two-hour hands-off measurement.

	η_{norm} [% W^{-1}]	d_{eff} [pm/V]
DGF	0.4	6.62[a]–9.01[b]
ZOF	0.1	3.82[a]–5.20[b]
BK[c]	0.2–0.4	6.5–9[d]
BK_{max}[e]	1.4–2.7	6.5–9[d]
LS[f]	0.2–0.3	6.5–9[d]
LS_{max}[g]	0.6–1.2	6.5–9[d]

[a]Calculated from Eq. (2) for $L = 10$ mm
[b]Calculated from Eq. (2) for $L = 5.4$ mm
[c]From Ref. [5] with $L = 5.4$ mm and $h(0, 0.25) = 0.27$
[d]Estimate from Raicol Crystals Ltd.: $d_{\text{eff}} = 6.5$–9 pm/V
[e]From Ref. [5] with $L = 10$ mm and $h(0, 2.84) = 1.07$
[f]From Ref. [6] with $L = 5.4$ mm
[g]From Ref. [6] with $L = 10$ mm

TABLE 1 Measured and theoretical efficiencies and nonlinearities of the PPKTP crystal for type-I QPM SHG at 810 nm

The effective nonlinear coefficient was specified by the manufacturer of the crystal to be $d_{\text{eff}} = 6.5$–9 pm/V. From these values we may estimate the expected and optimal normalized efficiencies. Our results are collected in Table 1. The table contains values of the expected and optimal efficiencies as calculated with the original theory by Boyd and Kleinman [5] for focused Gaussian beams (BK and BK_{max}) and with the extended Boyd–Kleinman analysis of Librecht and Simons (LS and LS_{max}) for elliptical beams [6]. As apparent from Table 1, the DGF SHG is in good agreement with the theoretical estimations. The discrepancy between the measured SHG efficiency and the calculated maximum efficiencies may be attributed to several factors, such as beam ellipticity, focal spot size, deviation of the DGF laser intensity distribution from the ideal Gaussian, spectral band width, linear absorption of the crystal, imperfect periodic poling, and the true value of the effective nonlinear coefficient.

The nonlinear coefficient d_{33} used here may be estimated from d_{eff} [11]: $d_{33} = d_{\text{eff}}\,\pi m/2\sin(\pi m D)$, where D is the duty cycle, i.e. the ratio between the size of the inverted ferroelectric domain and the QPM grating, and m is the order of the QPM. Assuming an optimal structure, i.e. a 50% duty cycle and with $m = 1$, we obtain $d_{33} = 14.6$ pm/V (8.9 pm/V) with (without) DGF. The value of d_{33} obtained with the DGF laser is in good agreement with commonly accepted values [10, 12] of $d_{33} = 16.9$–18.5 pm/V.

4 Conclusion

In conclusion, we have demonstrated a novel scheme for a high-power BAL-based blue–UV light source. The efficiency of the SHG process was measured and compared to theoretical estimations. A maximum of 0.6 mW was obtained at 405 nm corresponding to a normalized efficiency of $\eta_{\text{norm}} = 0.4\%\,\text{W}^{-1}$. This is several orders of magnitude more than is obtained with the freely running laser and a factor of four more than is obtained with ZOF alone. This shows that simultaneous improvement of the spatial and temporal coherence is imperative in order to use high-power LDs in SHG. The second-harmonic power may be increased by using an AR-coated BAL or a BAL with higher output power than the one used in this work. We may also use a grating with lower diffraction efficiency, thus increasing the amount of power in the zeroth-order output beam. Furthermore, the results may be improved by implementing the nonlinear crystal in a resonator-enhanced setup. Operating the pump laser in pulsed mode will also lead to an increase in SHG efficiency due to the high peak powers. Initial experiments indicate that the power of the pump laser may be increased by at least a factor of seven by direct current modulation [7]. This corresponds to an increase of a factor of 50 of the second-harmonic light. In comparison, by pulsing the 405-nm InGaN-based diodes from Nichia, the peak power is expected to increase by a factor of two as compared to the power of the continuous-wave device (personal communication, I. Toshiaki, Nichia Corp., Japan). This system has great potential for efficient generation of UV light, since the DGF scheme also applies to lower, e.g. red, wavelengths.

ACKNOWLEDGEMENTS The authors thank Christian Pedersen from Risø National Laboratory for useful discussions. This research was financially supported by the Danish Technical Research Council via Grant No. 9901433.

REFERENCES

1 L. Goldberg, L.E. Busse, D. Mehuys, Appl. Phys. Lett. **63**, 2327 (1993)
2 T. Laurila, R. Hernberg, Appl. Phys. Lett. **83**, 845 (2003)
3 S. Nakamura, J. Cryst. Growth **201–202**, 290 (1999)
4 E. Samsøe, P.E. Andersen, S. Andersson-Engels, P.M. Petersen, Opt. Express **12**, 609 (2004)
5 G.D. Boyd, D.A. Kleinman, J. Appl. Phys. **19**, 3597 (1968)
6 F.M. Librecht, J.A. Simons, IEEE J. Quantum Electron. **11**, 850 (1975)
7 E. Samsøe, *Laser Diode Systems for Photodynamic Therapy and Medical Diagnostics*, Ph.D. Thesis, Lund Institute of Technology, Lund University, Sweden (2004)
8 P.M. Fishbane, S. Gasiorowicz, S.T. Thornton, *Physics for Scientists and Engineers, Extended Version* (Prentice-Hall, Englewood Cliffs, NJ, 1993)
9 C.J. Chang-Hasnain, J. Berger, D.R. Scifres, W. Streifer, J.R. Whinnery, A. Dienes, Appl. Phys. Lett. **50**, 1465 (1987)
10 V. Pasiskevicius, S. Wang, J.A. Tellefsen, F. Laurrell, H. Karlsson, Appl. Opt. **37**, 7116 (1998)
11 M.M. Fejer, G.A. Magel, D.H. Jundt, R.L. Byer, IEEE J. Quantum Electron. **28**, 2631 (1992)
12 W.P. Risk, T.R. Gosnell, A.V. Nurmikko, *Compact Blue–Green Lasers* (Cambridge University Press, 2003)